actuators

Article

An IDA-PBC Design with Integral Action for Output Voltage Regulation in an Interleaved Boost Converter for DC Microgrid Applications

Oscar Danilo Montoya [1,2,*], Federico Martin Serra [3], Walter Gil-González [4], Eduardo Maximiliano Asensio [3] and Jonathan Emmanuel Bosso [3]

1 Facultad de Ingeniería, Universidad Distrital Francisco José de Caldas, Bogotá 110231, Colombia
2 Laboratorio Inteligente de Energía, Universidad Tecnológica de Bolívar, Cartagena 131001, Colombia
3 Laboratorio de Control Automático (LCA), Facultad de Ingeniería y Ciencias Agropecuarias, Universidad Nacional de San Luis—CONICET, Villa Mercedes, San Luis 5730, Argentina; fmserra@unsl.edu.ar (F.M.S.); maxiasensio@gmail.com (E.M.A.); jnthnbss@gmail.com (J.E.B.)
4 Facultad de Ingeniería, Institución Universitaria Pascual Bravo, Campus Robledo, Medellín 050036, Colombia; walter.gil@pascualbravo.edu.co
* Correspondence: odmontoyag@udistrital.edu.co

Abstract: This paper describes the output voltage regulation control for an interleaved connected to a direct current (DC) microgrid considering bidirectional current flows. The proposed controller is based on an interconnection and damping passivity-based control (IDA-PBC) approach with integral action that regulates the output voltage profile at its assigned reference. This approach designs a control law via nonlinear feedback that ensures asymptotic stability in a closed-loop in the sense of Lyapunov. Moreover, the IDA-PBC design adds an integral gain to eliminate the possible tracking errors in steady-state conditions. Numerical simulations in the Piecewise Linear Electrical Circuit Simulation (PLECS) package for MATLAB/Simulink demonstrate that the effectiveness of the proposed controller is assessed and compared with a conventional proportional-integral controller under different scenarios considering strong variations in the current injected/absorbed by the DC microgrid.

Keywords: nonlinear passivity-based control design; interleaved boost converter; voltage regulation; direct current microgrids; classic PI design

Citation: Montoya, O.D.; Serra, F.M.; Gil-González, W.; Asensio, E.M.; Bosso, J.E. An IDA-PBC Design with Integral Action for Output Voltage Regulation in an Interleaved Boost Converter for DC Microgrid Applications. *Actuators* **2022**, *11*, 5. https://doi.org/10.3390/act11010005

Academic Editors: Oscar Barambones, Jose Antonio Cortajarena and Patxi Alkorta

Received: 22 November 2021
Accepted: 26 December 2021
Published: 29 December 2021

1. Introduction

Recent advances in power electronics from high- to low-power voltages for direct current (DC) applications make owning DC distribution networks in medium and low voltage levels with high levels of efficiency possible [1,2]. Since DC distribution does not require reactive power and frequency concepts to operate, energy losses are inferior in these systems when compared with its traditional alternating current (AC) counterparts [3]. Generally, a DC microgrid can be composed of multiple devices interconnected to the main regulated bus [4,5], which include renewable generation, batteries, linear loads (i.e., resistances), and constant power loads, requiring specialized controllers to ensure a stable operation in a closed-loop [6,7]. The interconnection of these devices is executed with power electronic converters that allow the controlling of each device into their operative range, ensuring secure working. Some of the most conventional converters for DC microgrid applications include buck [8], boost [6], buck-boost [9], non-inverting buck-boost [10], and Cuk converters [11]. The main characteristic of these devices is that, usually, due to the presence of commutated devices inside of their electrical circuits, they generate nonlinear dynamic models that complicate the usage of classical linear controllers such as PI (Proportional-Integral) and feedback designs [10,12].

The importance of the power electronic converters is illustrated in the development of the electricity service using DC microgrids (see Figure 1) [13]. In this paper, we explore the possibility of employing an interleaved boost converter for output voltage regulation in DC microgrid applications, considering that the grid current can be positive or negative as a function of the amount of renewable energy available and the total power consumption [14].

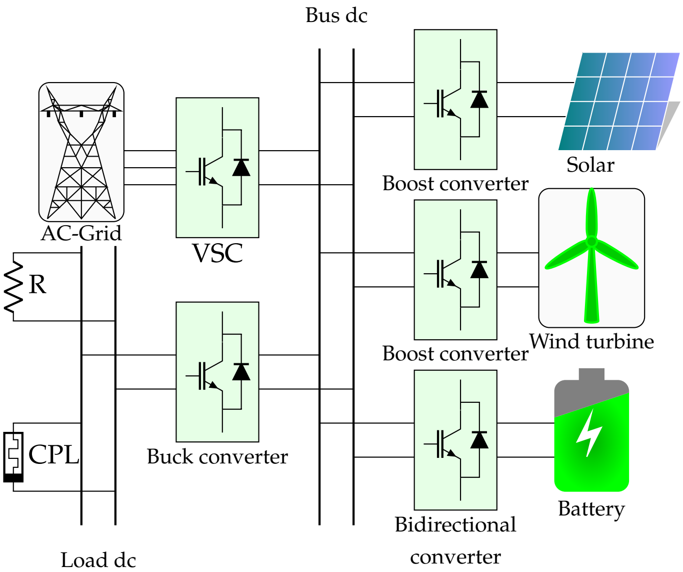

Figure 1. A typical DC microgrid with various sources and loads.

The interleaved boost converter is selected to support the voltage profile due to its simple structure and high capacity for transporting current owing to each parallel connection of inductor branches, allowing bidirectional current flow. Hence, this converter topology is ideal for applications that involve battery charging/discharging operating conditions, maintaining the voltage profile in the DC microgrid as consistently as possible [15].

Multiple control approaches have been applied to the interleaved boost converter for DC microgrid applications, some of which are discussed below. The authors of [14] present the design of a conventional PI controller in its digital version to control the current injected/absorbed by a battery pack to ensure reliable operation. Numerical and experimental validations of the proposed PI controller reveal that the objective of control is fulfilled by the PI design; however, the authors do not compare their control design with other control techniques, which do not permit measuring the effectiveness of their approach in terms of settling times and signal overshoots. The authors of [16] propose the application of the high-speed version of the model's predicted control approach to support voltage in DC microgrids using an interleaved boost converter with four inductive branches. Numerical simulations and experimental validations depicted the effectiveness of the proposed controller when compared with the classical model predictive and PI controllers. Cervantes et al. in [17] presented a time-varying switching-based controller for an interleaved boost converter composed of two inductor branches for electric vehicle applications. The proposed controller selects the switching surfaces distinctively for each interleaved converter cell to guarantee both maximum current and voltage ripple. Numerical simulations and experimental validations confirm its effectiveness in regulating the output voltage for a resistive load; however, the main flaw of this research was that the authors did not provide comparisons with other control methodologies. The authors of [18] present the application of the discrete-time inverse optimal control to an interleaved boost converter with two branches. They used the Euler approximation and the bilinear Tustin discretization to obtain a linear equivalent discrete model of the network, facilitating the control design via the inverse optimal control approach. Numerical results demonstrate the effectiveness of the proposed controller in supporting constant voltage to resistive loads independent of their variations; however, no comparisons with classical or nonlinear methodologies were provided in this study. Additional control methodologies include sliding control [19,20], exact state-feedback control [21,22], Hamiltonian-based controllers [23,24], neural and fuzzy controller designs [25,26], and [27], among others.

Based on the previous revision of the state-of-the-art regarding control applications for interleaved boost converters in this research, we present the following contributions:

i. The application of the IDA-PBC controller to the interleaved boost converter for output voltage regulation in DC microgrids with variable injected/demanded current: to improve the IDA-PBC design's performance, an integral action is added using the passive output of the system that does not affect the stability properties in closed-loop and allows eliminating the steady-state errors introduced by possible unmodeled dynamics;
ii. The proposed controller owns the advantage of not depending on the parameters of the interleaved boost converter which makes its robustness parametric variations.
iii. Select the current references through the inductor to maintain a balanced operation at each branch for positive and negative references.

Note that numerical validations in the Piecewise Linear Electrical Circuit Simulation (PLECS) simulation environment demonstrate the effectiveness and robustness of the proposed control design to maintain the output voltage on its reference with minimum overshoots when compared with the classical PI design that presents higher oscillations in the voltage output, which are also transferred to the inductor currents.

The remainder of this paper is structured as follows: Section 2 presents the dynamical modeling of the interleaved boost converter using averaging modeling theory; Section 3 describes the general IDA-PBC design for power electronic converters with port-Hamiltonian representation as well as the extension of this controller to include integral actions. Section 4 specifies all the numerical validations of the proposed controller with its corresponding comparisons with the conventional PI design for multiple operative conditions in the DC microgrid terminals that include positive and negative current inputs and voltage reference variations. Finally, Section 5 lists the main findings of this research as well as some possible future works.

2. Average Modeling for an Interleaved Boost Converter

An interlaced boost converter is featured by having two converters operate in parallel, which switch at the same frequency with a phase-shift between the control inputs [28]. The phase shift allows a decrease in the ripple of the input and output waveforms and a lower harmonic content in the converter [16]. The interleaved boost converter is widely used for battery charge/discharge because of its simplicity and high conversion rate.

Figure 2 illustrates the interleaved boost converter, where v_b and i_b are the battery voltage and current, i_{L_1} and i_{L_2} are the currents through the inductances, and v_{dc} is the capacitor voltage. The parameters L_1, L_2, and C are the two inductances and capacitance, respectively. The duty cycles $d_{1,2} \in [0,1]$ control the states of the converter and $\bar{d}_{1,2}$ are their negative values. The control objective in this paper corresponds with the voltage support in v_{dc} terminals for positive and negative variations of the input current (charging/neutral/discharging operative conditions on the battery). The currents through the inductors must have the same values to balance the operation of the converter and, thus, lead to a decrease in the ripple of current waveforms through the converter.

Applying Kirchhoff's laws over the interleaved boost converter presented in Figure 2 and defining the state variables and control signals as: $x = [x_1,\ x_2,\ x_3]^\top = [i_{L_1},\ i_{L_2},\ v_{dc}]^\top$, $u = [u_1,\ u_2]^\top = [d_1,\ d_2]^\top$, the following dynamic model is yielded:

$$
\begin{aligned}
L_1\dot{x}_1 &= v_b - x_3(1-u_1),\\
L_2\dot{x}_2 &= v_b - x_3(1-u_2),\\
C\dot{x}_3 &= x_1(1-u_1) + x_2(1-u_2) - i_{\text{bus}}.
\end{aligned} \tag{1}
$$

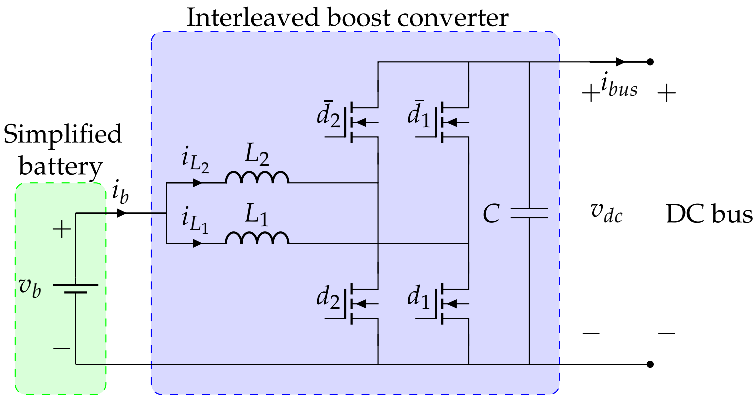

Figure 2. Electrical connection of an interleaved boost converter.

The dynamic model (1) can be rewritten in port-Hamiltonian (pH) structure as follows:

$$Q\dot{x} = (J - R)\frac{\partial H(x)}{\partial x} + G(x)u + \zeta, \tag{2}$$

where $\zeta = [v_b,\ v_b,\ -i_{\text{bus}}]^\top$ is the external inputs; $Q = Q^\top = \text{diag}(L_1,\ L_2,\ C) \succ 0$ is a positive definite matrix with the elements that store energy in the converter; R is the dissipation matrix, which takes a null form when no resistive effects on inductors are considered, that is, $R = 0_{3\times3}$; $H(x)$ is a storage function (with a similar form to an energy storage function with normalized structure) of the system which is widely known as the Hamiltonian function, note that $\frac{\partial H(x)}{\partial x} = x$. $J = -J^\top$ is a skew-symmetry matrix; and $G(x)$ is the input matrix. The form of these functions and matrices is presented below:

$$H(x) = \frac{1}{2}\left(x_1^2 + x_2^2 + x_3^2\right),\ J = \begin{bmatrix} 0 & 0 & -1 \\ 0 & 0 & -1 \\ 1 & 1 & 0 \end{bmatrix},\ G(x) = \begin{bmatrix} x_3 & 0 \\ 0 & x_3 \\ -x_1 & -x_2 \end{bmatrix}.$$

Remark 1. *The main characteristic of the dynamical model (2) is that it is possible to obtain a nonlinear feedback controller via passivity-based control that ensures the closed-loop stability in the sense of Lyapunov. This can be made by selecting an adequate desired dynamics to sustain its pH properties as presented in [29].*

The design of the passivity-based controller with integral action is detailed in the next section.

3. IDA-PBC Design

3.1. Assignable Equilibrium Point

To stabilize any dynamical system via control around an equilibrium point, it is necessary to ensure its existence is independent of its stability properties [29,30]. In the case of DC micrograds in steady-state operating conditions, this equilibrium must be constant [10], that is, $\dot{x} = 0$, which implies that the dynamical system (2) must fulfill that:

$$(J - R)\frac{\partial H(x^\star)}{\partial x^\star} + G(x^\star)u^\star + \zeta = 0, \tag{3}$$

from (3), the following steady state operative conditions are reached:

$$u_1^\star = 1 - \frac{v_b}{x_3^\star}, \tag{4}$$

$$u_2^\star = 1 - \frac{v_b}{x_3^\star}, \tag{5}$$

$$x_1^\star + x_2^\star = \frac{x_3^\star}{v_b} i_{\text{bus}}. \tag{6}$$

In the case of the current reference for each inductor, the main challenge in the literature is to identify an adequate current balance in interleaved converters [14]; for this reason, we have chosen $x_1^\star = x_2^\star$, which from (5) implies that the reference for each inductor current is defined below:

$$x_1^\star = x_2^\star = \frac{1}{2}\frac{x_3^\star}{v_b} i_{\text{bus}}. \tag{7}$$

Remark 2. *Observe that the control inputs $u_1^\star$ and $u_2^\star$ are defined as a function of the desired variable $x_3^\star$ (see Equations (4) and (5)), since this is the desired control objective, that is, to maintain the voltage value of the DC microgrid in its reference value independent of the current variations [14].*

3.2. Classical IDA-PBC Design

The main idea of the IDA-PBC design is to redefine the closed-loop dynamics of a physical system by exploiting its passivity properties [31]. For this purpose, the closed-loop dynamics of the system can be selected with the following form:

$$Q\dot{x} = (J_d - R_d)\frac{\partial H_d(\tilde{x})}{\partial \tilde{x}}, \tag{8}$$

where J_d and R_d are the desired interconnection and damping matrices which are skew-symmetry and positive definite, respectively. Note that these matrices are adjusted to cancel some undesired interconnections in the open loop and inject sufficient damping to stabilize the system [29]. $H_d(\tilde{x})$ is the desired Hamiltonian function, which must be positive definite to ensure asymptotic stability in the sense of Lyapunov for the error state variables $\tilde{x} = x - x^\star$.

To determine the closed-loop controller, we equate the open loop dynamics (2) with the desired dynamics (8), which produces the following partial differential equation:

$$(J - R)\frac{\partial H(x)}{\partial x} + G(x)u + \zeta = (J_d - R_d)\frac{\partial H_d(\tilde{x})}{\partial \tilde{x}}, \tag{9}$$

which is easily solvable if we adequately select the interconnection matrix J_d, desired damping matrix R_d, and Hamiltonian function $H_d(\tilde{x})$. The selection of these matrices and the Hamiltonian function are the following:

$$J_d = J_a + J,\ R_d = R_a + R,\ H_d(\tilde{x}) = \frac{1}{2}\tilde{x}^\top \tilde{x},$$

where

$$J_a = \begin{bmatrix} 0 & 0 & 0 \\ 0 & 0 & 0 \\ 0 & 0 & 0 \end{bmatrix},\ R_a = \begin{bmatrix} R_1 & 0 & 0 \\ 0 & R_2 & 0 \\ 0 & 0 & R_3 \end{bmatrix}.$$

With the aforementioned definitions, it is possible to obtain the general control laws u_1 and u_2 from the first two equations of (9), which generates the following results:

$$u_1 = \frac{x_3^\star - v_b - R_1(x_1 - x_1^\star)}{x_3}, \tag{10}$$

$$u_2 = \frac{x_3^\star - v_b - R_2(x_2 - x_2^\star)}{x_3}. \tag{11}$$

Additionally, the third equation of (9) generates the following algebraic equation relating all the state variables and references:

$$\begin{gathered}(v_b - x_3^\star)(x_1 + x_2) + R_1 x_1(x_1 - x_1^\star) + R_2 x_2(x_2 - x_2^\star) \\ x_3 R_3(x_3 - x_3^\star) + x_3(x_1^\star + x_2^\star) = x_3 i_{\text{bus}}.\end{gathered} \tag{12}$$

Remark 3. *Once the system dynamical system (2) has been stabilized with the IDA-PBC using control laws (10) and (11), we can observe that in steady state conditions, Equations (10)–(12) take the form defined in Equations (4)–(7)—which confirms that the system have reached the desired operative point.*

To ascertain that the proposed controller has asymptotic stability in closed-loop, let us consider the candidate Lyapunov function as the desired Hamiltonian function, that is, $V(\tilde{x}) = \frac{1}{2}\tilde{x}^\top Q\tilde{x}$, which is a positive definite and $V(0) = 0$. If we consider the time derivative of this function, then, the following result yields:

$$\begin{aligned}\dot{V}(\tilde{x}) &= \tilde{x}^\top Q\dot{x}, \\ &= \tilde{x}^\top (J_d - R_d)\tilde{x}, \\ &= -\tilde{x}^\top R_d \tilde{x} < 0,\end{aligned} \tag{13}$$

which confirms that the desired dynamical system (9) is asymptotically stable in the sense of Lyapunov, that is, $x \to x^\star$ as $t \to \infty$.

3.3. IDA-PBC Redesign with Integral Action

The usage of an IDA-PBC design with integral action is necessary to eliminate possible steady-state errors introduced by unmodeled dynamics in the original systems, such as resistive effects in inductors, parasite resistances in capacitors, or energy losses in forced-commutated switches, among others [6,29].

To formulate the general IDA-PBC with integral action, let us consider the following augmented dynamical system:

$$\begin{bmatrix} Q\dot{x} \\ \dot{z} \end{bmatrix} = \begin{bmatrix} (J_d - R_d) & -G(x) \\ G^\top(x) & 0 \end{bmatrix} \begin{bmatrix} \frac{\partial H_d(\tilde{x})}{\partial \tilde{x}} \\ \frac{\partial H_z(z)}{\partial z}, \end{bmatrix} \tag{14}$$

where $G^\top(x)\frac{\partial H_d(\tilde{x})}{\partial \tilde{x}}$ is the passive output of the desired dynamical system [32]; K_i is a diagonal positive definite matrix that contains the integral grains, z is the vector of auxiliary state variables, and $H_z(z)$ is the Hamiltonian function defined in the set of auxiliary variables, which is defined as $H_z(z) = \frac{1}{2}z^\top K_i z$.

To confirm that the augmented dynamical system (14) is stable in the sense of Lyapunov, let us consider the following candidate Lyapunov function:

$$W(\tilde{x}, z) = V(\tilde{x}) + H_z(z). \tag{15}$$

Note that $W(\tilde{x}, z)$ is a positive definite function and $W(0, 0) = 0$ only for the point in the origin of coordinates; now, taking the time derivative of (15), the following result is produced:

$$\begin{aligned}\dot{W}(\tilde{x}, z) &= \tilde{x}^\top Q\dot{x} + z^\top K_i \dot{z}, \\ &= \tilde{x}^\top (J_d - R_d)\tilde{x} - \tilde{x}^\top G(x) K_i z + z^\top K_i G^\top(x)\tilde{x}, \\ &= -\tilde{x}^\top R_d \tilde{x} < 0. \end{aligned} \tag{16}$$

Note that (16) ensures that the augmented dynamical system (14) is stable in the sense of Lyapunov.

Now, observe that the closed-loop dynamics will be defined by equaling the first row of (14) with the open-loop dynamics (2), which produces the following partial differential equation.

$$(J - R)\frac{\partial H(x)}{\partial x} + G(x)u + \zeta = (J_d - R_d)\frac{\partial H_d(\tilde{x})}{\partial \tilde{x}} - G(x)K_i \frac{\partial H_z(z)}{\partial z}. \tag{17}$$

If we solve (17) for the control laws u_1 and u_2, then, the following results are reached:

$$u_1 = \frac{x_3^\star - v_b - R_1\left(x_1 - x_1^\star\right)}{x_3} - K_1 z_1, \tag{18}$$

$$u_2 = \frac{x_3^\star - v_b - R_2(x_2 - x_2^\star)}{x_3} - K_2 z_2, \tag{19}$$

where z_1 and z_2 defines the integral components of the controller. These components are calculated with the second row of (14) as presented below:

$$z_1 = \int x_3(x_1 - x_1^\star)dt - \int x_1(x_3 - x_3^\star)dt, \tag{20}$$

$$z_2 = \int x_3(x_2 - x_2^\star)dt - \int x_2(x_3 - x_3^\star)dt. \tag{21}$$

Remark 4. *The control inputs u_1 and u_2 in (18) and (19) with the integral components (20) and (21) define the general IDA-PBC with integral action to stabilize the interleaved boost converter in the desired reference to support voltage in DC microgrid applications independent of the variations of the external input, that is, i_{bus}.*

4. Numerical Validation

This section exhibits the performance of the IDA-PBC with integral action implemented in an interleaved boost converter to regulate the output voltage under different load conditions. The proposed controller is validated in the test system displayed in Figure 2, and its parameters are outlined in Table 1. Moreover, the IDA-PBC is also compared to the conventional PI controller [14]. The simulations are conducted in the PLECS software, and the sample time for the proposed controller is configured in 10 µs.

Table 1. Interleaved boost converter parameters.

Element	Variable	Value	Element	Variable	Value	Element	Variable	Value
Battery Voltage	v_b	24 V	Bus Voltage	v_{dc}	48 V	Inductor	L_1, L_2	330 mH
Switching frequency	f_q	2 kHz	Capacitor	C	44 µF			

It is worth mentioning that the PLECS software is a complete interface to simulate electrical grids predominantly composed of power electronic converters that allow designing controllers using block diagrams or functions [33]. The main advantage of this simulation tool is that it works under the Simulink solution environment and can be easily implemented in real-time simulators for Hardware in the Loop applications [34].

The dynamic response of the proposed control is evaluated against different disturbances generated with current steps in the DC bus to emulate the charging/discharging processes of the converter. These current steps are 1 A, 1.5 A, and 2 A, both positives, and negatives with 30 ms intervals, as depicted in Figure 3.

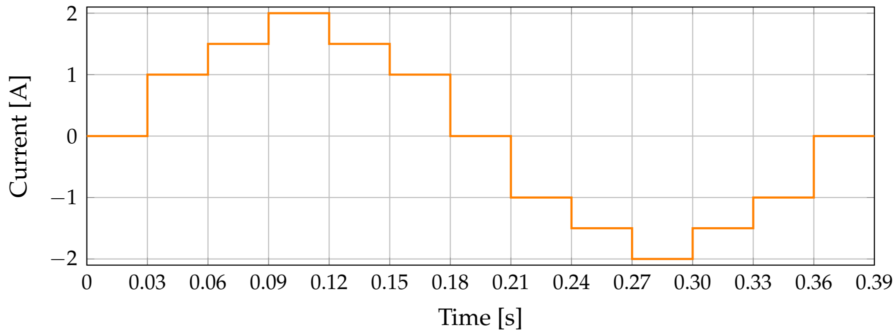

Figure 3. Variations in the input signal i_{bus}.

Figure 4 illustrates the output voltage of the interleaved boost converter under different DC current steps, in Figure 4a for the conventional PI controller and in Figure 4b for the proposed IDA-PBC.

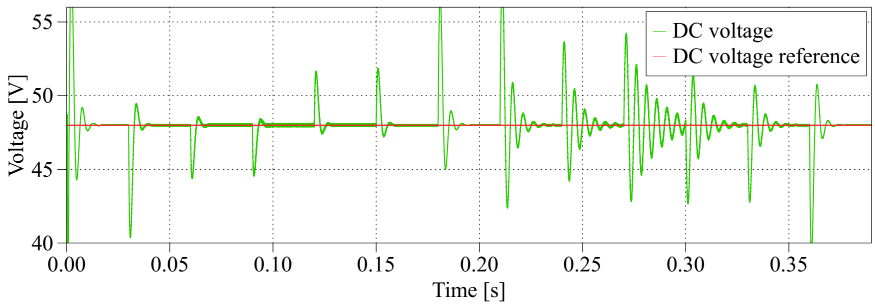

(**a**) PI controller

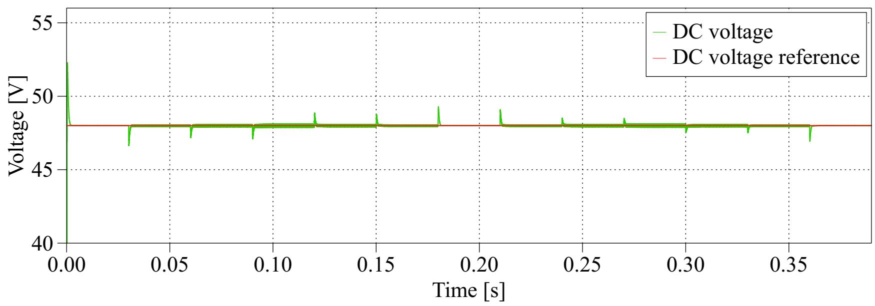

(**b**) IDA-PBC.

Figure 4. The dynamic response of output voltage of the interleaved boost converter under different DC current steps.

Comparing Figure 4a,b, it can be noted that the IDA-PBC adequately regulates the output voltage of the interleaved boost converter under different DC current steps, while conventional PI has higher oscillations, higher voltage overshoots, and it is slower than the proposed controller. This behavior is exacerbated by the the DC bus current's negative values. This analysis is supported by comparing the voltage overshoot and settling time. The voltage overshoot in the worst case for the proposed controller is 1.3 V, while the conventional PI controller is 8 V. For the settling time, the proposed controller requires 3 ms to stabilize in the worst case while the conventional PI controller needs 40 ms.

Figure 5 unveils the currents in the interleaved boost converter, DC current bus, and battery current. Figure 5a,b present the currents in the interleaved boost converter, DC current bus, and battery current when the conventional PI controller and IDA-PBC are used, respectively.

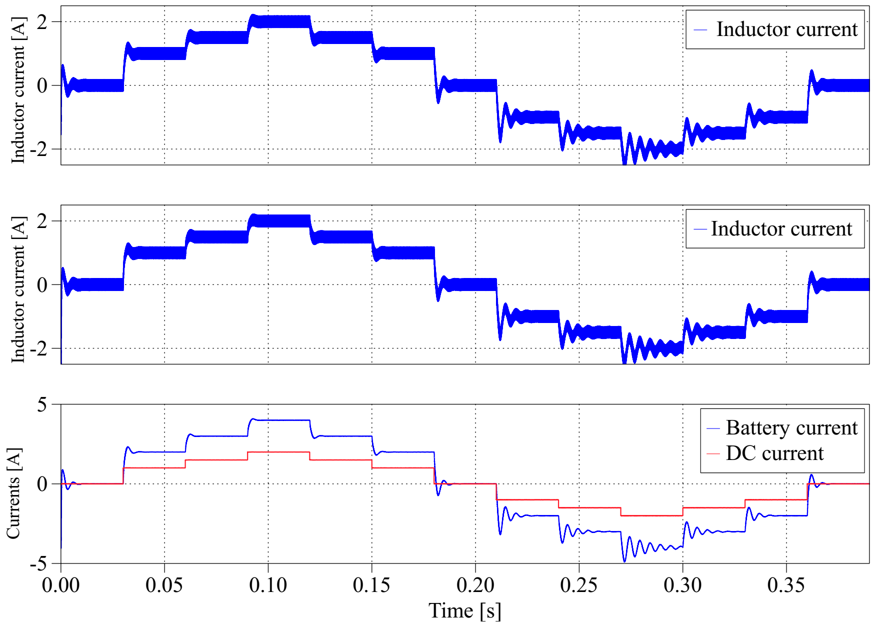

(**a**) PI controller

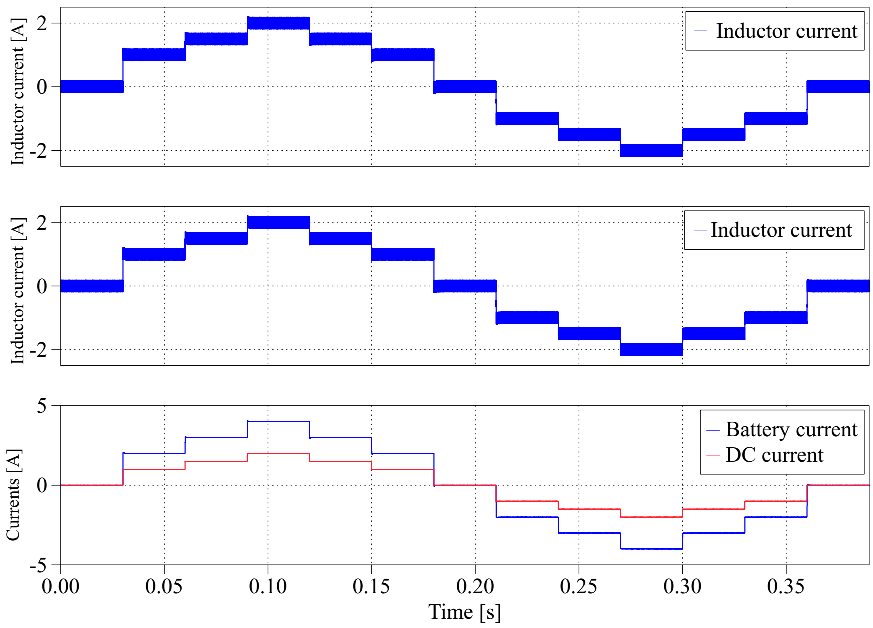

(**b**) IDA-PBC.

Figure 5. The dynamic response of currents associated with the interleaved boost converter under different DC current steps.

Comparing the behavior of the currents associated with the interleaved boost converter in Figure 5a,b, it is evident that the inductor currents stabilize faster when the IDA-PBC is implemented. Further, the conventional PI controller presents oscillation when the DC current bus has negative references, indicating that the interleaved boost may become unstable for large negative reference values on the DC current bus.

Figure 6 depicts control inputs for the proposed controller and PI control. For both controllers, the control inputs do not overshot their limits. Additionally, comparing the dynamic response of the voltage output with control inputs, it is observed that both exhibit the same behavior, that is, they are directly proportional.

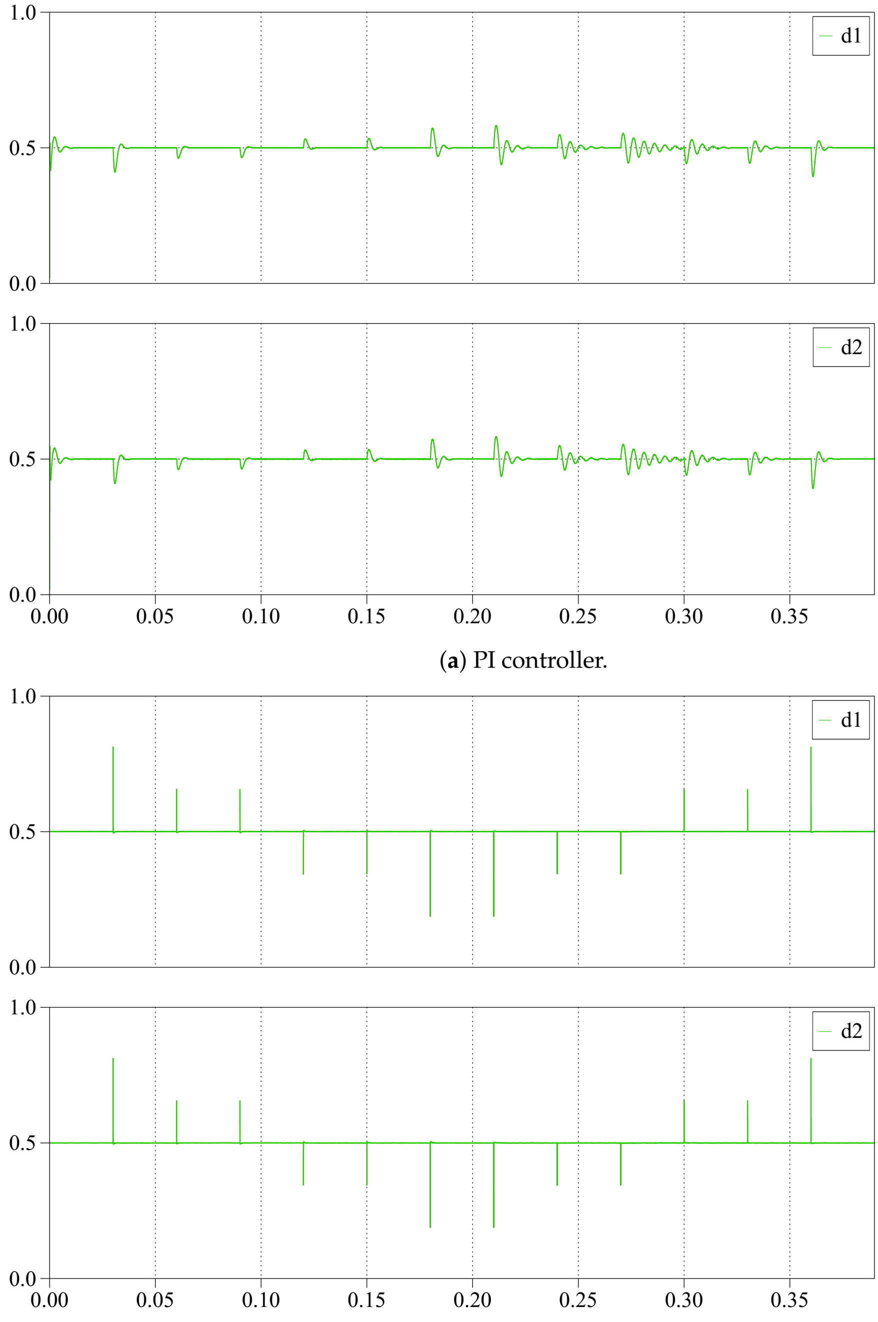

(**a**) PI controller.

(**b**) IDA-PBC.

Figure 6. The dynamic response of control inputs with the interleaved boost converter under different DC current steps.

Now, the performance of the proposed control for different voltage value references is examined as displayed in Figure 7.

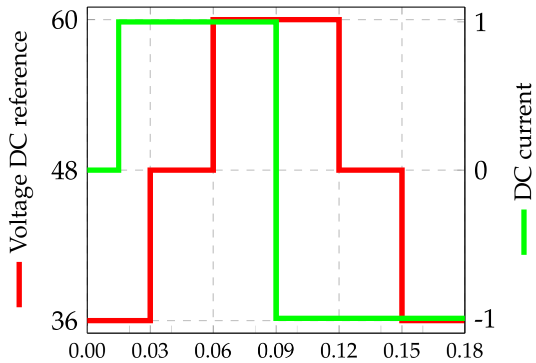

Figure 7. Different voltage DC references.

Figure 8 depicts the output voltage of the interleaved boost converter under different voltage DC references. Figure 8a,b show the output voltages of the interleaved boost converter when the conventional PI and IDA-PBC controllers are implemented.

Comparing Figure 8a,b, it can be perceived that the output voltage of the interleaved boost converter is correctly followed when the IDA-PBC is employed, whereas the output voltage has oscillations when the conventional PI controller is used. Therefore, the proposed controller continues presenting a better performance than the conventional PI controller. This is supported by comparing the voltage overshoot and settling time. The maximum voltage overshoot occurs when the current changes from 1 to -1 (time 0.9 s), while for the proposed controller, it is 0.775 V and 23.674 V for the conventional PI controller. For the settling time, the proposed controller requires 12 ms to stabilize in the worst case while the conventional PI controller needs 40 ms.

Figure 9 illustrates the currents associated with the interleaved boost converter. The currents in both inductors, DC bus and battery, are displayed in Figure 9a,b when the conventional PI and the IDA-PBC controller are implemented.

The difference in the behavior of the currents associated with the interleaved boost converter continues to be maintained as seen in Figure 5, establishing that the proposed IDA-PBC controller performs better than the conventional PI.

Figure 10 depicts the control inputs for the proposed controller and PI control when the interleaved boost converter is under different DC voltage and current steps. For both controllers, the control inputs do not overshoot their limits. The voltage output dynamics depict the same behavior as that of the control inputs, implying that the voltage output response is directly proportional to the control inputs.

It is worth emphasizing that, during the physical implementation of the proposed IDA-PBC controller, an adequate tuning process of the proportional and integral gains is mandatory to obtain the expected dynamical behavior. However, classical tuning techniques are not applicable due to the interleaved boost converter and IDA-PBC design generating a nonlinear feedback model [35]. For this reason, it is recommended to generate a mesh with multiple combinations of these gains and use an optimization technique to tune these using a performance index, which can be the mean square error or another [10].

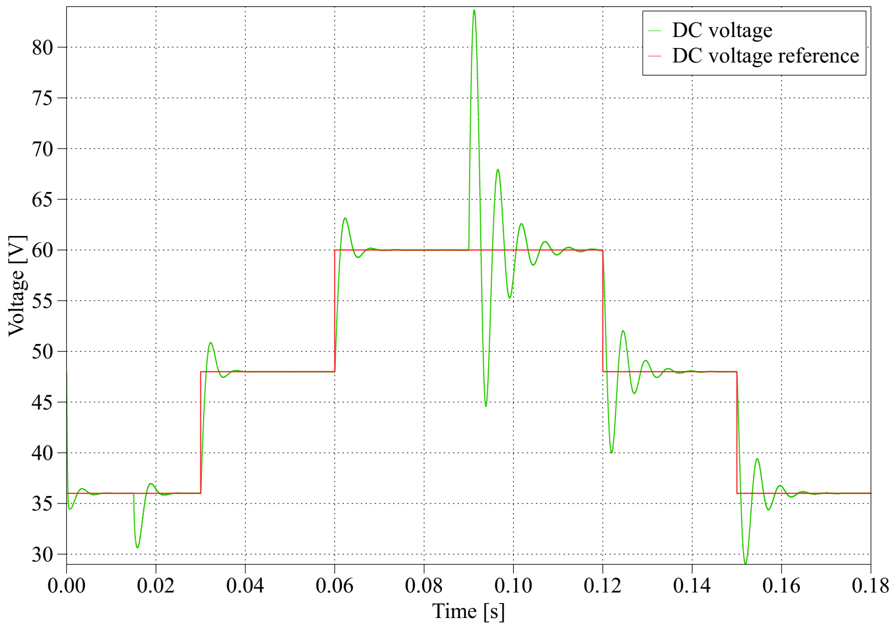

(**a**) PI controller.

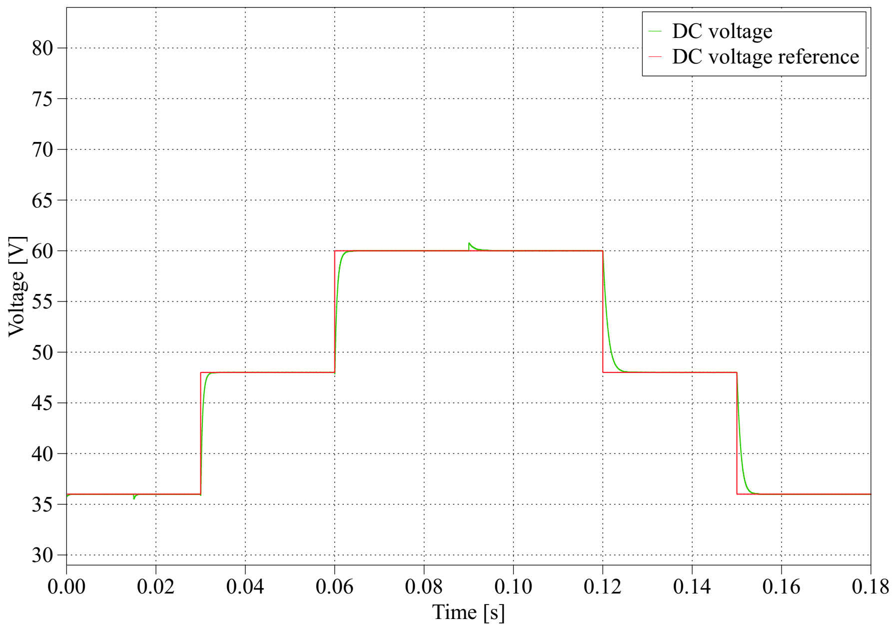

(**b**) IDA-PBC.

Figure 8. The dynamic response of output voltage of the interleaved boost converter under different DC voltage and current steps.

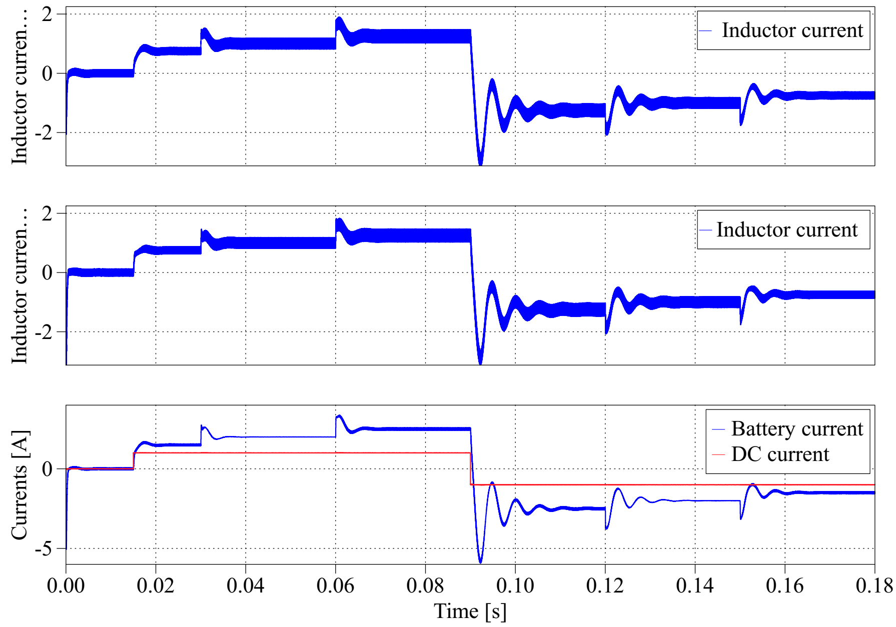

(**a**) PI controller.

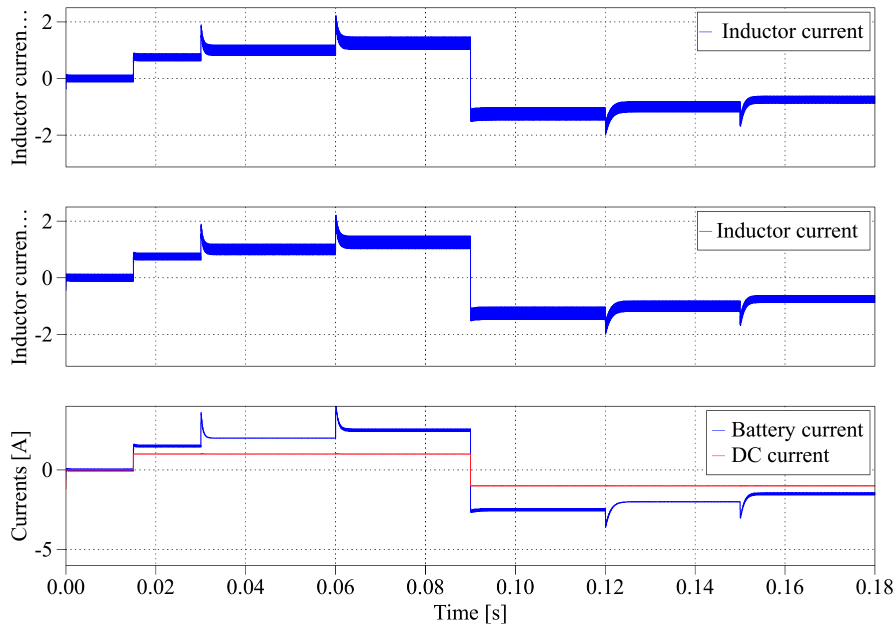

(**b**) IDA-PBC

Figure 9. The dynamic response of currents associated with the interleaved boost converter under different DC voltage and current steps.

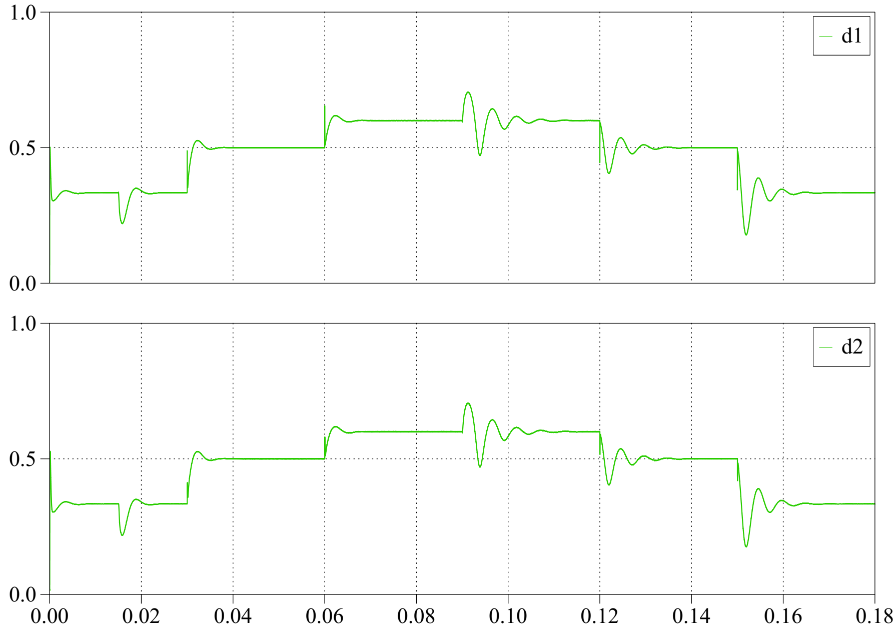

(**a**) PI controller.

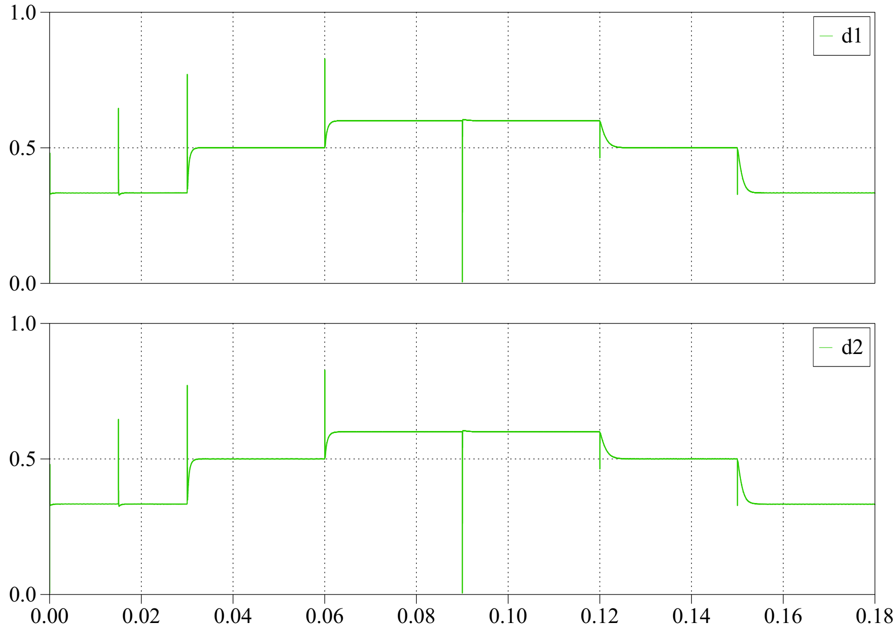

(**b**) IDA-PBC.

Figure 10. The dynamic response of control inputs with the interleaved boost converter under different DC voltage and current steps.

5. Conclusions and Future Works

A passivity-based control applied to the interleaved boost converter or output voltage regulation in DC microgrids with variable injected/demanded current was proposed in this paper. The passivity-based control is performed using the interconnection and damping assignment, which takes advantage of the system's dynamic in open-loop to design a control law guaranteeing the system's stability in closed-loop. Additionally, an integral action was included in the IDA-PBC design to enhance the performance of the proposed controller, thus, eliminating the steady-state errors introduced by possible unmodeled dynamics. This integral action did not affect the stability properties since it maintains the passive output of the system. The proposed controller was assessed under different simulation scenarios and compared with a conventional PI controller, exhibiting better performance than the PI controller. This was supported by comparing the integral of the voltage overshoot and settling time.

Future works could be developed from the following studies: (i) the application of the IDA-PBC with integral action to DC-DC converters, such as quadratic buck and boost converters; (ii) develop a complete experimental comparison among nonlinear control designs applied to the interleaved boost converter with a special focus on exact feedback linearization, inverse optimal control, and Lyapunov-based approaches; and (iii) extend the IDA-PBC design to the interleaved boost converter under the presence of nonlinear constant power loads.

Author Contributions: Conceptualization, methodology, software, and writing—review and editing, O.D.M., F.M.S., W.G.-G., E.M.A. and J.E.B. All authors have read and agreed to the published version of the manuscript.

Funding: This work was supported in part by the Centro de Investigación y Desarrollo Científico de la Universidad Distrital Francisco José de Caldas under grant 1643-12-2020 associated with the project: "Desarrollo de una metodología de optimización para la gestión óptima de recursos energéticos distribuidos en redes de distribución de energía eléctrica".

Institutional Review Board Statement: Not applicable.

Informed Consent Statement: Not applicable.

Data Availability Statement: No new data were created or analyzed in this study. Data sharing is not applicable to this article.

Acknowledgments: This work has been derived from the doctoral research project: "Análisis, operación y control de convertidores para la integración de recursos energéticos distribuidos en redes eléctricas aisladas" presented by the student Oscar Danilo Montoya to the Doctoral program of the Engineering Faculty at Universidad Nacional de Rio Cuarto as a partial requirement for the PhD in Engineering Sciences.

Conflicts of Interest: The authors declare no conflict of interest.

References

1. Lana, A.; Mattsson, A.; Nuutinen, P.; Peltoniemi, P.; Kaipia, T.; Kosonen, A.; Aarniovuori, L.; Partanen, J. On Low-Voltage DC Network Customer-End Inverter Energy Efficiency. *IEEE Trans. Smart Grid* **2014**, *5*, 2709–2717. [CrossRef]
2. Montoya, O.D.; Gil-González, W.; Serra, F.M.; Angelo, C.H.D.; Hernández, J.C. Global Optimal Stabilization of MT-HVDC Systems: Inverse Optimal Control Approach. *Electronics* **2021**, *10*, 2819. [CrossRef]
3. Garces, A. Uniqueness of the power flow solutions in low voltage direct current grids. *Electr. Power Syst. Res.* **2017**, *151*, 149–153. [CrossRef]
4. Justo, J.J.; Mwasilu, F.; Lee, J.; Jung, J.W. AC-microgrids versus DC-microgrids with distributed energy resources: A review. *Renew. Sustain. Energy Rev.* **2013**, *24*, 387–405. [CrossRef]
5. Lotfi, H.; Khodaei, A. AC Versus DC Microgrid Planning. *IEEE Trans. Smart Grid* **2017**, *8*, 296–304. [CrossRef]
6. Magaldi, G.L.; Serra, F.M.; de Angelo, C.H.; Montoya, O.D.; Giral-Ramírez, D.A. Voltage Regulation of an Isolated DC Microgrid with a Constant Power Load: A Passivity-based Control Design. *Electronics* **2021**, *10*, 2085. [CrossRef]
7. Serra, F.M.; Angelo, C.H.D. Control of a battery charger for electric vehicles with unity power factor. *Trans. Energy Syst. Eng. Appl.* **2021**, *2*, 32–44. [CrossRef]
8. Solsona, J.A.; Jorge, S.G.; Busada, C.A. Nonlinear Control of a Buck Converter Which Feeds a Constant Power Load. *IEEE Trans. Power Electron.* **2015**, *30*, 7193–7201. [CrossRef]
9. Salimi, M.; Siami, S. Cascade nonlinear control of DC-DC buck/boost converter using exact feedback linearization. In Proceedings of the 2015 4th International Conference on Electric Power and Energy Conversion Systems (EPECS), Sharjah, United Arab Emirates, 24–26 November 2015; IEEE: Piscataway, NJ, USA, 2015. [CrossRef]
10. Gil-González, W.; Montoya, O.D.; Restrepo, C.; Hernández, J.C. Sensorless Adaptive Voltage Control for Classical DC-DC Converters Feeding Unknown Loads: A Generalized PI Passivity-Based Approach. *Sensors* **2021**, *21*, 6367. [CrossRef]
11. Ramos-Paja, C.A.; Gonzalez-Motoya, D.; Villegas-Seballos, J.P.; Serna-Garces, S.I.; Giral, R. Sliding-mode controller for a photovoltaic system based on a Cuk converter. *Int. J. Electr. Comput. Eng. (IJECE)* **2021**, *11*, 2027. [CrossRef]
12. Jin, P.; Li, Y.; Li, G.; Chen, Z.; Zhai, X. Optimized hierarchical power oscillations control for distributed generation under unbalanced conditions. *Appl. Energy* **2017**, *194*, 343–352. [CrossRef]

13. Iskender, I.; Genc, N. Power Electronic Converters in DC Microgrid. In *Power Systems*; Springer International Publishing: Berlin/Heidelberg, Germany, 2019; pp. 115–137. [CrossRef]
14. Quintero, C.E.; Pérez, S.A.; Ceballos, J.P.V.; González-Montoya, D.; Garcés, S.S. Design and Digital Control of an Interleaved Boost Converter for Battery Charge/Discharge. *Tecnológicas* **2021**, *24*, e1556. (In Spanish) [CrossRef]
15. He, L.; Lin, Z.; Tan, Q.; Lu, F.; Zeng, T. Interleaved High Step-Up Current Sharing Converter with Coupled Inductors. *Electronics* **2021**, *10*, 436. [CrossRef]
16. Hausberger, T.; Kugi, A.; Eder, A.; Kemmetmüller, W. High-speed nonlinear model predictive control of an interleaved switching DC/DC-converter. *Control. Eng. Pract.* **2020**, *103*, 104576. [CrossRef]
17. Cervantes, I.; Mendoza-Torres, A.; Garcia-Cuevas, A.; Perez-Pinal, F. Switched control of interleaved converters. In Proceedings of the 2009 IEEE Vehicle Power and Propulsion Conference, Dearborn, MI, USA, 7–11 September 2009; IEEE: Piscataway, NJ, USA, 2009. [CrossRef]
18. Kumar, S.S.; Kanimozhi, G. A nonlinear control technique for interleaved boost converter. In Proceedings of the 2016 10th International Conference on Intelligent Systems and Control (ISCO), Coimbatore, India, 7–8 January 2016; IEEE: Piscataway, NJ, USA, 2016. [CrossRef]
19. Cid-Pastor, A.; Giral, R.; Calvente, J.; Utkin, V.I.; Martinez-Salamero, L. Interleaved Converters Based on Sliding-Mode Control in a Ring Configuration. *IEEE Trans. Circuits Syst. I Regul. Pap.* **2011**, *58*, 2566–2577. [CrossRef]
20. Tiwari, A.; Jaga, O.; Soni, S.S. Sliding mode controller based interleaved boost converter for fuel cell system. In Proceedings of the 2017 Recent Developments in Control, Automation & Power Engineering (RDCAPE), Noida, India, 26–27 October 2017; IEEE: Piscataway, NJ, USA, 2017. [CrossRef]
21. Gkizas, G.; Amanatidis, C.; Yfoulis, C.; Stergiopoulos, F.; Giaouris, D.; Ziogou, C.; Voutetakis, S.; Papadopoulou, S. State-feedback control of an interleaved DC-DC boost converter. In Proceedings of the 2016 24th Mediterranean Conference on Control and Automation (MED), Athens, Greece, 21–24 June 2016; IEEE: Piscataway, NJ, USA 2016. [CrossRef]
22. González, A.; López-Erauskin, R.; Gyselinck, J. Analysis, modeling, control and operation of an interleaved three-port boost converter for DMPPT systems including PV and storage at module level. *Heliyon* **2019**, *5*, e01402. [CrossRef] [PubMed]
23. Olmos-Lopez, A.; Guerrero, G.; Arau, J.; Aguilar, C.; Yris, J.C. Passivity-based control for current sharing in PFC interleaved boost converters. In Proceedings of the 2011 Twenty-Sixth Annual IEEE Applied Power Electronics Conference and Exposition (APEC), Fort Worth, TX, USA, 6–11 March 2011; IEEE: Piscataway, NJ, USA, 2011. [CrossRef]
24. Zhou, H.; Khambadkone, A.M.; Kong, X. A Passivity Based Control with Augmented Integration for an Interleaved Current Fed Full Bridge Converter as a Front End for Fuel Cell Source. In Proceedings of the 2007 IEEE Industry Applications Annual Meeting, New Orleans, LA, USA, 23–27 September2007; IEEE: Piscataway, NJ, USA, 2007. [CrossRef]
25. Bharathi, M.; Kirubakaran, D. Solar powered closed-loop controlled fuzzy logic-based three-stage interleaved DC-DC boost converter with an inverter. *Int. J. Adv. Intell. Paradig.* **2016**, *8*, 140. [CrossRef]
26. Sunarno, E.; Sudiharto, I.; Nugraha, S.D.; Qudsi, O.A.; Eviningsih, R.P.; Raharja, L.P.S.; Arifin, I.F. A Simple And Implementation of Interleaved Boost Converter For Renewable Energy. In Proceedings of the 2018 International Conference on Sustainable Energy Engineering and Application (ICSEEA), Tangerang, Indonesia, 1–2 November 2018; IEEE: Piscataway, NJ, USA, 2018. [CrossRef]
27. Barhoumi, E.; Belgacem, I.B.; Khiareddine, A.; Zghaibeh, M.; Tlili, I. A Neural Network-Based Four Phases Interleaved Boost Converter for Fuel Cell System Applications. *Energies* **2018**, *11*, 3423. [CrossRef]
28. Gonzalez, W.J.G.; Bocanegra, S.Y.; Serra, F.M.; Bueno-López, M.; Magaldi, G.L. Control Methods for Single-phase Voltage Supply with VSCs to Feed Nonlinear Loads in Rural Areas. *Trans. Energy Syst. Eng. Appl.* **2020**, *1*, 33–47. [CrossRef]
29. Serra, F.M.; Angelo, C.H.D.; Forchetti, D.G. Interconnection and damping assignment control of a three-phase front end converter. *Int. J. Electr. Power Energy Syst.* **2014**, *60*, 317–324. [CrossRef]
30. Herrera-Pérez, J.J.; Garcés-Ruiz, A. Análisis de estabilidad de convertidores de segundo orden con la metodología de optimización de suma de polinomios cuadráticos. *Trans. Energy Syst. Eng. Appl.* **2020**, *1*, 49–58. (In Spanish) [CrossRef]
31. Serra, F.M.; Angelo, C.H.D. IDA-PBC controller design for grid connected Front End Converters under non-ideal grid conditions. *Electr. Power Syst. Res.* **2017**, *142*, 12–19. [CrossRef]
32. Donaire, A.; Junco, S. On the addition of integral action to port-controlled Hamiltonian systems. *Automatica* **2009**, *45*, 1910–1916. [CrossRef]
33. Asadi, F.; Eguchi, K. *Simulation of Power Electronics Converters Using PLECS®*; Elsevier: Amsterdam, The Netherlands, 2020. [CrossRef]
34. Frivaldsky, M.; Morgos, J.; Prazenica, M.; Takacs, K. System Level Simulation of Microgrid Power Electronic Systems. *Electronics* **2021**, *10*, 644. [CrossRef]
35. Morales, J.A.; Castro, M.A.; Garcia, D.; Higuera, C.; Sandoval, J. IDA-PBC Controller Tuning Using Steepest Descent. In *Numerical and Evolutionary Optimization—NEO 2017*; Springer International Publishing: Berlin/Heidelberg, Germany, 2018; pp. 158–170. [CrossRef]